Coulomb Friction Crawling Model Yields Linear Force–Velocity Profile

Ziyou Wu[1]
Department of Electrical Engineering
and Computer Science,
University of Michigan,
Ann Arbor, MI M48105
e-mail: wuziyou@umich.edu

Dan Zhao
Department of Mechanical Engineering,
University of Michigan,
Ann Arbor, MI 48105 Michigan
e-mail: danzhaoy@umich.edu

Shai Revzen
Assistant Professor
Department of Electrical Engineering
and Computer Science,
University of Michigan,
Ann Arbor, MI 48105
e-mail: shrevzen@umich.edu

Conventional wisdom would have it that moving mechanical systems that dissipate energy by Coulomb friction have no relationship between force and average speed. One could argue that the work done by friction is constant per unit of distance travelled, and if propulsion forces exceed friction, the net work is positive, and the system accumulates kinetic energy without bound. We present a minimalistic model for legged propulsion with slipping under Coulomb friction, scaled to parameters representative of single kilogram robots and animals. Our model, amenable to exact solutions, exhibits nearly linear ($R^2 > 0.96$) relationships between actuator force and average speed over its entire range of parameters, and in both motion regimes, it supports. This suggests that the interactions inherent in multilegged locomotion may lead to governing equations more reminiscent of viscous friction than would be immediately obvious. [DOI: 10.1115/1.4042696]

Keywords: locomotion, friction, dynamics

1 Introduction

The ability to move through space is both the quintessential property of animals and one of the most desirable features of modern robots. However, our machines move very differently from our animal cousins. Most terrestrially mobile machines use wheels or treads, which maintain a continuous path of contact with the ground, whereas most animals rely on legs coming into intermittent contact with the environment to produce motion. Inasmuch as legged robots are used at all, much research has been focused on bipedal robots close to the size of humans, yet arguably the most successful group of legged animals on land are arthropods, all of whom utilize six or more legs and contact the ground at three or more points at (almost) all times.

Such multilegged locomotion is fundamentally different from both bipedal and wheeled locomotion. By using legs with intermittent ground contact, multilegged animals can move over discontinuous substrates. In addition, thanks to having many simultaneous points of contact rather than the single point of contact that bipeds often have, multilegged animals can tolerate significant slipping on the ground. For example, our group has recently shown that the feet (tarsi) of *Blaberus discoidalis* cockroaches running on a paper surface[2] spend about 20% of their entire motion in the lab frame slipping backward while in contact with the ground. In fact, it quickly became clear to us that as more and more legs are in contact with the ground it becomes harder to ensure that they all move in compatible ways to ensure nonslip contact, and slipping becomes inevitable in our robots. Thus, we were brought to the question of how to best model multilegged locomotion *with slipping*.

In this paper, we aim to provide a partial answer to this question. In particular, we show an emergent relationship among friction, actuation, collisions, and finite body size, which suggests that even when frictional contacts are well modeled by the classical Coulomb friction model [1,2], the average relationship between actuation force and body velocity looks remarkably similar to viscous friction [3]. We demonstrate this result with an overly simplistic model of locomotion with slipping, which is simple enough to allow us to analyze its solutions exhaustively. We also compare this model with a slightly more elaborate and physically plausible model, the results of which we only study numerically.

We begin by describing and motivating our sliding locomotion model in Sec. 2. In Sec. 3, we present the results of simulating the model over a range of parameters surrounding those applicable to small robots and animals. In Sec. 4, we solve for average force and velocity in a closed form. The instantaneous mass swapping explained in Sec. 2 is somewhat physically implausible, and so in Sec. 5, we present the results from a more physical model of mass swapping, which we analyze numerically. We follow by discussing these results in Sec. 6, where we hazard some guesses as to the cause and broader implications of having a force–velocity rather than a force–acceleration relationship.

2 Sliding Locomotion Model

Rather than confounding the effects of slipping with those of intermittent contact, we chose to model a uniaxial motion in a continuous sliding contact. Our model was inspired by the sort of shuffling that gait people sometimes employ on ice or other slippery surfaces, whereby they shift their weight over one leg, slide the other leg to a new position, and repeat, alternating the weight-bearing leg. Alternatively, this can be thought of as an inchworm gait on a slippery surface.

2.1 Mechanical Model. Consider two point masses with an actuator of finite length between them (see Fig. 1) operating at a constant force pushing them apart. Each of these masses represents a single leg, with the magnitude of the mass representing the loading on that leg. When the distance between two masses reaches a predetermined maximum, a perfectly plastic collision occurs. The positions of the two masses are swapped, representing a reversal of the leg loading, and the force flips sign to pull the masses together. Once they reach a minimal distance, they collide to create a plastic collision again, swap positions, the direction of force switches, and the cycle repeats. (A discussion of a more physical model of mass swapping can be found in Sec. 5.)

The equation of motion of the system is as follows:

$$m\ddot{x} = F_t \operatorname{sgn}(x - y) - f_m \tag{1}$$

$$M\ddot{y} = -F_t \operatorname{sgn}(x - y) - f_M \tag{2}$$

[1]Corresponding author.

Contributed by the Applied Mechanics Division of ASME for publication in the Journal of Applied Mechanics. Manuscript received December 7, 2018; final manuscript received January 31, 2019; published online March 5, 2019. Assoc. Editor: Ahmet S. Yigit.

[2]Elmer's 900803 Foam Board, Elmer's Products Inc., Atlanta GA.

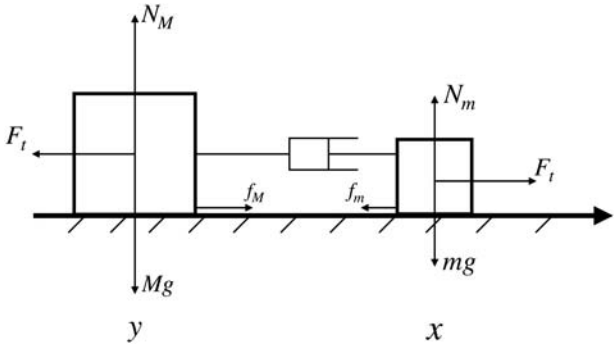

Fig. 1 Schematic representation of the mechanical model. *M* and *m* are the larger and smaller point masses, respectively, with *y* and *x* their positions. The friction forces acting on the point masses are f_m and f_M. F_t is the actuator force, which is positive when pushing the masses apart and negative when pulling them together. *g* is the gravitational acceleration.

We assume the Coulomb friction model for the contact forces [4]. In the Coulomb friction model, friction force is proportional to the normal load when velocity is not 0. When velocity is 0, the friction force can take any value between 0 and a static friction force proportional to the normal load.

This can be modeled using the following equations:

$$f = \begin{cases} \mu N \operatorname{sgn}(v) & \text{slipping (dynamic friction)} \\ F_e & \text{nonslip (static friction); } |F_e| < \mu_s N \end{cases} \tag{3}$$

where μ is the dynamic friction coefficient, μ_s is the static friction coefficient, F_e is the external force, and N is the normal force. Both masses are taken as point mass with state vector $[x, \dot{x}]^T$ and $[y, \dot{y}]^T$, respectively. The distance between the masses is bounded above and below by L_{max} and L_{min}, respectively. When either distance limit is reached, it is enforced by a perfectly plastic collision, which renders equal the velocity of both masses:

$$\dot{x}^+ = \dot{y}^+ = \frac{m\dot{x}^- + M\dot{y}^-}{m+M} \tag{4}$$

Immediately after the masses collide, they instantaneously swap positions, i.e. the precollision state $[x, \dot{x}^-, y, \dot{y}^-]^\mathsf{T}$ gives rise to the postcollision state $[y, \dot{y}^+, x, \dot{x}^+]^\mathsf{T}$.

This last model assumption factors out the details of exactly how the moving system redistributes load over its legs and merely captures the notion that the leg load alternates between the two possible configurations.

2.2 Dynamic Analysis. Holding actuation force at constant magnitude, alternately extending and contracting the actuator through its full stroke length, the system seems to approach a periodic motion and asymptote to a limiting average speed (see Fig. 2) in the entire parameter range we explored. Although the system is easy to define in terms of the states of the point masses, it is easier to analyze in terms of the center of mass (CoM) position $c := (mx + My)/(m + M)$ and the position difference $d := y - x$. In these coordinates, it is evident that the actuator does no work on c—it is an "internal force"—and all work on the CoM is done by the friction forces. Since we are using the Coulomb friction model, once the actuator force is sufficient to get the smaller mass m out of static friction, the actuator will successfully expand and contract to its full extent at any CoM speed. If the motion approaches a limit cycle in $[d, \dot{d}]^\mathsf{T}$, the average speed of the CoM over a long simulation will converge to the speed at the limit cycle v_{ss} of (5).

$$v_{ss} = \frac{\text{Distance traveled in one steady cycle}}{\text{Duration of one steady cycle}} \tag{5}$$

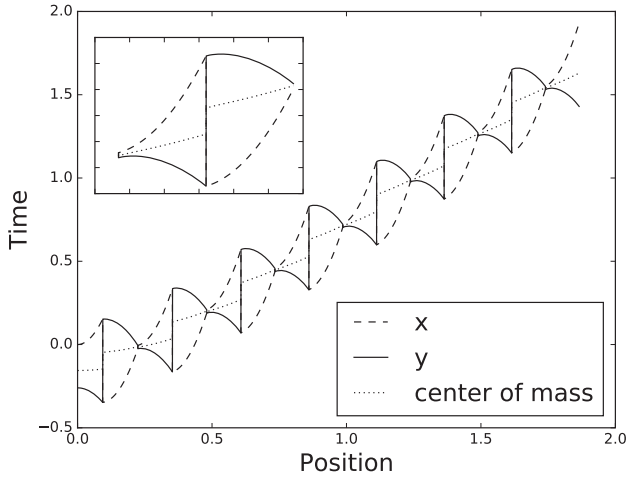

Fig. 2 Position of *m*, *M*, and the center of mass versus time in an example simulation. Parameter choices followed Sec. 3. Force $F_t = 45\operatorname{sgn}(x - y)$ *N*; dynamic friction coefficient was $\mu = 1$. The positions of *m* (dashed line), *M* (solid line), and center of mass $(mx + My)/(m + M)$ (dotted line) over time are shown. The graph at the left upper corner shows an enlarged cycle starting at $y - x = L_{min}$. The accelerations of *m* and *M* are always opposite to each other. They accelerate until the length constraint at L_{min} and L_{max} stops them, and they instantly swap their positions. The position swap causes a jump of the center of mass. Note that for the first two cycles of motion, the CoM is noticeably changing average speed, which quickly asymptotes to its limiting value.

For our numerical simulations, we ran the simulations until relative difference of averaged v_{ss} between two consecutive cycles decreased to within 10^{-4}.

3 Numerical Simulation Results

We chose simulation parameters appropriate for a small robot or mid-size vertebrate such as a rabbit. We took the masses to be $m = 1$ kg, $M = 1.5$ kg. The mass ratio M/m specifies the instantaneous center of mass displacement when masses are swapped, which becomes $0.2d$ for these values. The minimum and maximum distance between two masses were taken to be $L_{min} = 0.02$ m and $L_{max} = 0.5$ m, respectively. The range of dynamic friction coefficient μ we explored was 0.05–1. The range of input force F was set from μmg—the minimal force needed to escape static friction—up to 5 Mg—enough to produce a greater than $2g$ acceleration on the CoM.

In our simulation, we fix the actuator force to be a constant force with periodically changing directions, i.e., $F_t = F \operatorname{sgn}(x - y)$, where F is a constant input force and x and y are positions of m and M, respectively.[3] Without the loss of generality, we start at $d = L_{min} > 0$, and thus, m is to the right of M, and the masses are pushed apart. Because the masses swap their positions, the actuator is always either pushing or pulling the smaller mass m to the right (positive direction) and pushing or pulling the larger mass M to the left (negative direction). Mass M has better traction than m by having larger friction forces, due to its larger normal force on the substrate. Thus, the net friction force generated in this way can move the system in the positive direction.

3.1 Two Motion Regimes Arise. We fixed all the parameters and only change the absolute value of actuator force F by examining the changes induced in v_{ss}. Two fundamentally different motion regimes arose: regime I—when actuator force is only large enough to take small mass m out of its static friction cone,

[3] Attempting to allow the force to depend on d always lead to the highest v_{ss} with the force identically maximal, and so this was added as an assumption.

i.e., $f_m < F \leq f_M$, leading to the small mass moving against a static support offered by the large mass; and regime II—when actuator force is large enough to move both small and large masses $F > f_M$, leading to the large mass sliding in the opposite direction of the small mass.

For each input actuator force F, we observed a corresponding final steady-state velocity v_{ss} of the system. Figure 3 shows the relationship for $\mu = 1$ and $\mu = 0.2$, although a similar qualitative relationship exists for the entire range, we explored $0.05 \leq \mu \leq 1$.

For regime I, we explored the entire force range: $(\mu mg, \mu Mg)$. For regime II, we explored forces in the range $[\mu Mg, 5Mg]$, which represent a reasonable range of mass specific actuator force density for animals [5–7], electrically powered autonomous robots, and internal combustion engines [8,9].

Writing $v_{ss} = kF + b$, we also explored the relationship of k and b with μ following parameter choices in Sec. 3. The quadratic regression equation for k versus μ is $k = -1.9 \times 10^{-3}\mu^2 + 11 \times 10^{-3}$, with $R^2 = 0.99$. The linear regression equation for b versus μ is $b = 0.24\mu + 0.46$, with $R^2 = 0.99$.

3.1.1 Governing Relationship. Combining our numerical results, we found that the averaged steady-state velocity versus actuator force model for the system regime II can be empirically described by a single governing equation correct for actuator forces less than $5Mg$, and $0.05 \leq \mu \leq 1$.

Since the model we used has physical units, to obtain a more principled governing relationship, we first switched to a nondimensional form. Let $F := \tilde{f}\mu Mg$ and $v_{ss} := \tilde{v}\sqrt{Lg}$, where $\tilde{f}$ is the nondimensional force, in units of friction for the large mass, and $\tilde{v}$ is the nondimensional velocity, in units of the velocity reached in free fall over the maximal length of the actuator.

The nondimensional model is shown in (6), to two digits precision, and was constructed for $\tilde{f}$ between 1 and $5/\mu$.

$$\tilde{v} = 0.073\mu\left(1 - 0.178\mu^2\right)\tilde{f} + 0.11\mu + 0.20 \tag{6}$$

4 Exact Solution

Assuming the system will achieve a steady-state averaged velocity v_{ss}, we solved a closed-form solution for v_{ss} versus μ and F. We start from the dynamic motion Eqs. (1), (2), and recall $d := x - y$. We obtain the following equations:

$$m\ddot{x} = F\,\mathrm{sgn}(d) - \mu mg\,\mathrm{sgn}(\dot{x})$$
$$M\ddot{y} = -F\,\mathrm{sgn}(d) - \mu Mg\,\mathrm{sgn}(\dot{y})$$

Suppose, as we empirically observed, that each cycle starts from $d = L_{min}$ and account for the fact that this state appears immediately after a plastic collision, making the velocities of m and M equal. We obtain $\dot{x}_0 = \dot{y}_0 = \dot{c}_0$, where $\dot{c}_0$ is the velocity of CoM. We define, w.l.o.g., that this velocity's direction is positive. Due to the negative force on the large mass M, it first decelerates until its velocity goes to zero and then accelerates toward negative direction or remains

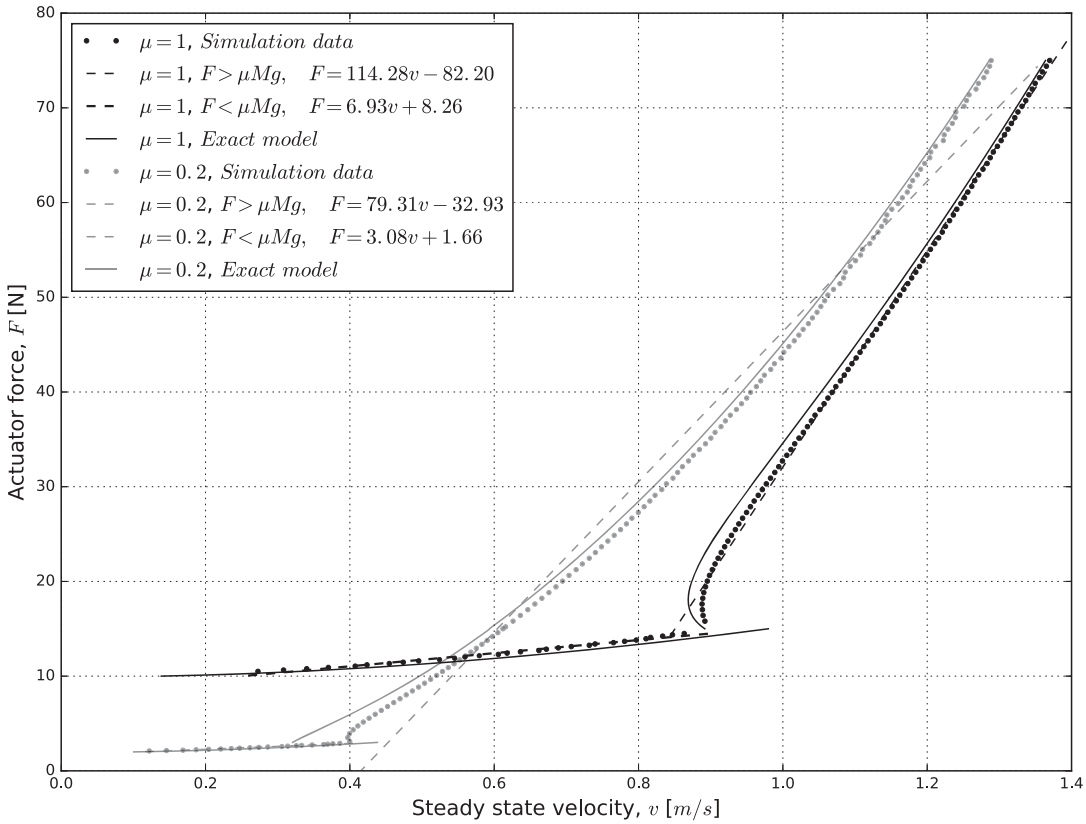

Fig. 3 Constant force versus steady-state velocity under Coulomb friction model, $\mu = 1$ and $\mu = 0.2$. We plotted simulation results for regime I where $F < \mu Mg$, with $\mu = 1$ (black dots) and with $\mu = 0.2$ (gray dots). These are close to their regression lines $\mu = 1$ (dashed black line) $R^2 = 0.99$ and $\mu = 0.2$ (dashed gray line) $R^2 = 0.99$. For regime II where $F > \mu Mg$, we plotted simulations for $\mu = 1$ (black dots) and $\mu = 0.2$ (gray dots). Each of these follows a nearly linear relationship different from that of the other force regime ($\mu = 1$ dashed black regression $R^2 = 1.0$ and $\mu = 0.2$ dashed gray regression $R^2 = 0.99$). We also plotted the exact solution as calculated in Sec. 4 when $\mu = 1$ (black solid line) and, $\mu = 0.2$ (gray solid line) for the entire motion regime. Our notable result is that in each regime, the F to v_{ss} relationship can be described fairly accurately as linear, as demonstrated by the high values of regression R^2. Note that intermediate values of μ interpolate those plotted and were omitted for clarity.

zero if F is not large enough to push it out of static friction. The motion is shown schematically in Fig. 4.

$$m\ddot{x} = F - \mu mg \tag{7}$$

$$M\ddot{y} = \begin{cases} -F - \mu Mg & \dot{y} > 0 \\ \min(-F + \mu Mg, 0) & \dot{y} \le 0 \end{cases} \tag{8}$$

The equation of motion for the CoM of the system in the first stage of Fig. 4 is $\ddot{c}_1 = -\mu g$. The time spent at first stage can be calculated from the time needed for M to achieve zero velocity, $t_1 = \mathcal{T}_1(\dot{c}_0) = \dot{c}_0/(F/M + \mu g)$. When $\dot{y} = 0$, the center of mass velocity becomes $\dot{c}_1 = \dot{c}_0 F/(F + \mu Mg)$.

Time t_2 is the time needed for the distance between m and M to reach the maximum length bound. It can be determined by a second-order equation (9), and the result of $t_2 = \mathcal{T}_2(\dot{c}_0)$ is a function of the initial CoM velocity.

$$L_{max} - L_{min} - \frac{1}{2}(\ddot{x} - \ddot{y}_1)t_1^2 = \dot{x}_{t_1} t_2 + (\ddot{x} - \ddot{y}_2)t_2^2 \tag{9}$$

Here, $\ddot{y}_1$ is the acceleration of M when $\dot{y} > 0$, and $\ddot{y}_2$ is the acceleration of M when $\dot{y} < 0$ as shown in Fig. 4 (the slope of solid line). They are calculated from (8).

Thus, the update rule for CoM velocity after each velocity cycle is as follows:

$$\dot{c}_2 = \frac{F}{F + \mu Mg}\dot{c}_0 + \frac{M - m}{M + m}\mu g + \mathcal{T}_2(\dot{c}_0) \tag{10}$$

By solving for the fixed point of this equation, we can get $\dot{c}_0$ as a function of F and μ, $\dot{C}_0(F, \mu)$. The averaged steady-state CoM velocity v_{ss} can be calculated by (11). The second term is the CoM position shift due to instantaneous swaps of two masses at L_{min} and L_{max}.

$$\mathcal{V}_{ss}(F, \mu) = \frac{2F + \mu Mg}{2(F + \mu Mg)}\dot{C}_0 + \frac{M - m}{m + M}\frac{L_{max} - L_{min}}{2(\mathcal{T}_1 + \mathcal{T}_2)} \tag{11}$$

The symbolic calculations were done in Mathematica.

4.1 Comparison With Governing Relationship. We compared our empirically derived governing relationship discussed in Sec. 3.1.1 with the analytical solution given in Sec. 4. The relative error of the model is below 5% except for small forces and low friction, where it grows to 11%.

Our results are best summarized by the examples in Fig. 3, showing v_{ss} versus F regressions, numerical model simulation results, and exact algebraic results for both motion regimes. One puzzling observation regarding this figure is the separation between exact and numerical curves. Decreasing integrator time-steps and requiring more stringent convergence from the numerical simulations bring these curves closer together—an observation that suggests that convergence to the limit cycle may be quite slow. However, these differences still remain somewhat puzzling.

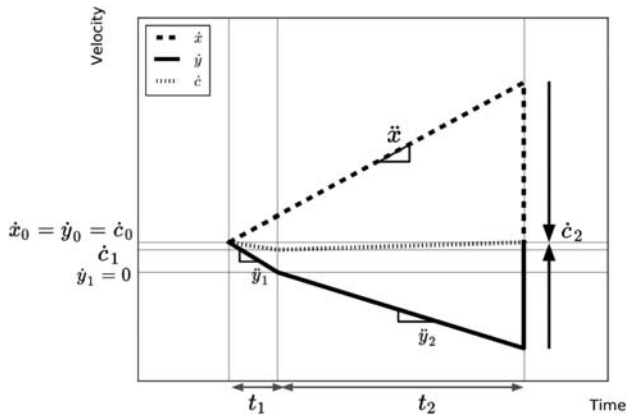

Fig. 4 Schematic of velocities within a cycle of regime II motion. We plotted the velocity of m (dashed line), M (solid line), and CoM (dotted line) in one velocity cycle. The initial value of these velocities are $\dot{x}_0 = \dot{y}_0 = \dot{c}_0$. t_1 is the time it takes for the velocity of M starting from $\dot{y}_0$ to decrease to 0. The velocity of the CoM at t_1 is $\dot{c}_1$. t_2 is the remaining time needed for distance between m and M to achieve maximum length bound. $\ddot{x}$ is the constant acceleration of m, and $\ddot{y}_1$, $\ddot{c}_1$, $\ddot{y}_2$, and $\ddot{c}_2$ are accelerations of M and CoM during time period t_1 and t_2. At the end of the cycle, velocities are reset by a second plastic collision (represented by two arrows).

5 Realistic Swapping Yields Similar Results

To make the model more realistic in mimicking an inchworm or a legged robot/animal shuffling, we modeled a mechanistic means for transferring the mass difference $\Delta m := M - m$ between the two point masses of the previous model. To do so, we postulated an internal force pushing Δm from one side to the other side, while the distance between the two end point masses is held constant. This is illustrated in Fig. 5. When the Δm mass reaches its destination, it collides in a plastic collision, and all three masses have zero relative velocity after collision.

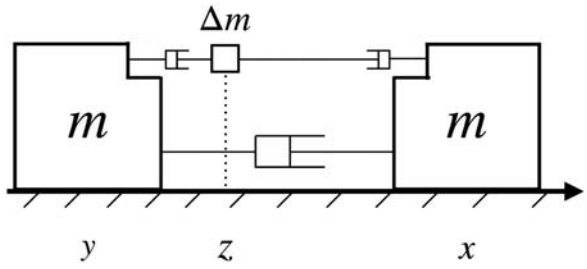

Fig. 5 Schematic representation of the mechanical model with a swapping mechanism. x, y, and z represent the position of each point mass.

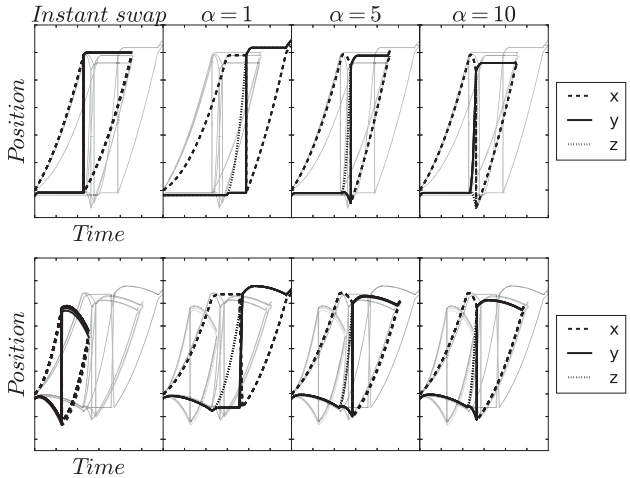

Fig. 6 Position of m, M, and Δm versus time within a cycle. We plotted these for the one mass moving regime (top, $F = 12N$) and two masses moving regime (bottom, $F = 20N$). The dynamic friction coefficient was $\mu = 1$. The positions of m (dashed line, x), M (solid line, y), and Δm (dotted line, z) plotted with time and position starting at the L_{min} collision are shown. We plotted four cycles, illustrating the rapid convergence to a limit cycle. To facilitate comparison, we plotted all conditions in each subplot with one condition highlighted (darker, with markers) and the others rendered de-emphasized (gray). We compared the instantaneous swap model (left column) and values of $\alpha = 1$, 5, 10 (second to fourth columns). Note that $m - m$ keeps its position during Δm swapping when $\alpha = 1$, whereas it moves backward when $\alpha = 5$, 10.

The equation of motion remains the same as (1) and (2) when the system is slipping and Δm is fixed on one of m. As our notation convention, we take the mass m with Δm as M and write its position as y. We denote the other m mass by x, and when Δm is in motion, it is always moving from x to y. Here afterward, we will refer to the two end point masses, while they are held at a constant distance, as the $m-m$ system. The relative movement between Δm and $m-m$ system can be described as follows. Taking $m-m$ as one object, its center is $c := (x+y)/2$. Suppose a force of $F_{\Delta m}$ is used to push Δm (whose position is denoted by z) against $m-m$, the equations of motion for the exchange of Δm are as follows:

$$2m\ddot{c} = \begin{cases} 0 & \text{if } \dot{c} = 0 \text{ and } |F_{\Delta m}| < \mu g(2m + \Delta m) \\ -F_{\Delta m} - \text{sgn}(\dot{c})\mu g(2m + \Delta m) & \text{else} \end{cases}$$

$$\Delta m\ddot{z} = F_{\Delta m}$$

5.1 Numerical Simulation. Following the same choice of parameters in Sec. 3, we use a nondimensional parameter α to give $F_{\Delta m} := \alpha F \, \text{sgn}(z-x)$ as the force pushing Δm from M to m, where F is the actuation force between m and M. In Fig. 6, we compare the cycle behavior between instant swap model and constant swapping force models with $\alpha = 1$, 5, 10 in both one mass moving and two mass moving regimes. The models are still asymptotic to a limiting periodic cycle, which vary slightly with α.

5.2 Four Motion Regimes Arise. With the parameters selected in Sec. 3, we found four motion regimes arising from two independent conditions. The first condition is discussed in Sec. 3.1, namely comparing actuation force F with μmg and μMg. It leads to either one or two masses in dynamic friction during the times $x-y$ changes. The second condition was comparing the total friction force of the system $\mu(2m+\Delta m)g$ with swapping force $F_{\Delta m}$. When moving sufficiently slowly, if $|F_{\Delta m}| \le \mu g \ (2m+\Delta m)$, the $m-m$ system first slowed down to a standstill position and stayed in that position until the end of Δm motion. If $|F_{\Delta m}| > \mu g \ (2m+\Delta m)$, the reaction force for moving Δm was large enough to pull the $m-m$ system out of friction cone during

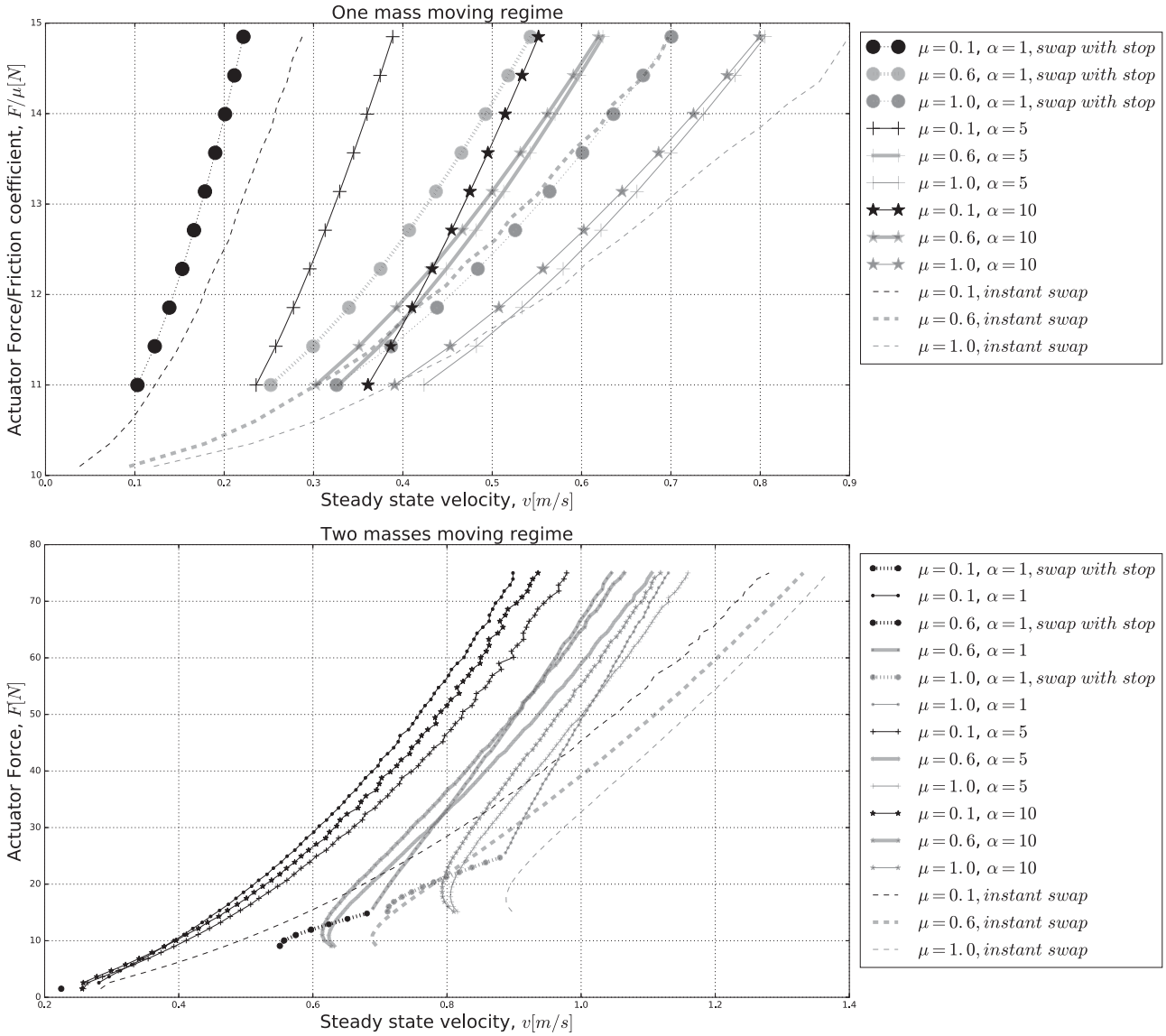

Fig. 7 Actuation force versus steady-state velocity under Coulomb friction model with constant swapping forces. We plotted the simulation results for friction coefficient $\mu = 1$ (black), $\mu = 0.6$ (thicker gray), and $\mu = 1.0$ (gray). For each μ, we plotted swapping forces $\alpha = 1$ (· marker), $\alpha = 5$ (+ marker), $\alpha = 10$ ($\star$ marker), and instant swap (dashed lines). We also plotted the new "stop during swap" motion regimes (larger round markers with dotted lines). All models are linear to an $R^2 > 0.99$ (single mass moving regime) and $R^2 > 0.96$ (two masses moving regime).

swapping and pushed it backward. For example, in Fig. 6, when $\alpha = 1$, $m - m$ slowed down and stopped during Δm swapping. When $\alpha = 5$, 10, $m - m$ slowed down and was eventually accelerating toward the negative direction during Δm swapping.

In Fig. 7, we plotted the relationships for $\mu = 0.1$, 0.6, 1.0, and swapping force coefficients $\alpha = 1$, 5, 10. The figure shows that a new "swap with stop" motion regime appears. Outside this new motion regime, the F to v relationship follows the same qualitatively nearly linear relationship similar to that for the instantaneous swap model.

6 Discussion

Our simulations and our analytic studies of the models we described brought us to a surprising conclusion: we conclude that the averaged velocity versus input force in Coulomb friction dominated motion is a linear relationship, at least for the parameter range governing small robots and animals. We observed this qualitative relationship to hold in both a simplified "instant-swap" model (Sec. 2) and a more physical weight redistribution model (Sec. 5).

The very existence of a linear relationship between force and velocity in a Coulomb friction governed system should come as a surprise, because once static friction is compensated for, the Coulomb friction model predicts a speed-independent dynamic friction. Thus, for example, in an idealized wheeled system without air resistance or a lubricant viscosity model, no upper limit on speed exists. Once the drive motor is strong enough to overcome internal friction, the wheeled system has a constant acceleration rather than a limiting velocity.

The appearance of a viscosity-like relationship out of simple dry friction interactions is somewhat reminiscent of the appearance of viscosity in statistical mechanics, where thermodynamic equilibrium and the associated viscous dissipation appear after only a small number of particle collisions.

It may also be that our observation can be understood in the light of a fundamental limit of friction-based locomotion: the CoM can never move faster relative to the ground than the body can change shape. If it did, all points of contact would be slipping in the direction of motion and therefore producing braking forces. Broadly speaking, the speed of shape change is associated with a kinetic energy, which must be developed by an actuation force acting over the length of the body. The relationship $mv^2 \propto F \cdot l$ suggests that v should scale as $F^{0.5}$, which is not wholly incompatible with the lower limit of friction $\mu = 0.1$ that we explored. However, if instead we assumed that the duration of force action is bounded, then $\Delta(mv) \propto F\Delta t$, and the shape change speed is linear with F. As both these limitations play a role in practice, a close to linear relationship may be inevitable regardless of the specifics of the friction model.

Acknowledgment

All authors were supported by ARO Grant Nos. W911NF-14-1-0573 and W911NF-17-1-0306 to Revzen. We thank S. Burden and the anonymous reviewer for their helpful comments.

References

[1] Coulomb, C. A., 1785, "Theorie des Machines Simples," Memoirs de Mathematique et de Physique de l'Academie Royale.

[2] Anh, L., and Belyaev, A., 2012, *Dynamics of Mechanical Systems with Coulomb Friction*, Springer Science & Business Media, Heidelberg, Germany.

[3] Reynolds, O., 1886, "On the Theory of Lubrication and Its Application to Mr. Beauchamp Tower's Experiments, Including an Experimental Determination of the Viscosity of Olive Oil," Philos. Trans. R. Soc. London, **177**, pp. 157–234, IV.

[4] Olsson, H., Åström, K. J., de Wit, C. C., Gäfvert, M., and Lischinsky, P., 1998, "Friction Models and Friction Compensation," Eur. J. Control, **4**(3), pp. 176–195.

[5] Alexander, R., 1985, "The Maximum Forces Exerted by Animals," J. Exp. Biol., **115**(1), pp. 231–238.

[6] Walter, R. M., and Carrier, D. R., 2007, "Ground Forces Applied by Galloping Dogs," J. Exp. Biol., **210**(2), pp. 208–216.

[7] Weyand, P. G., Sternlight, D. B., Bellizzi, M. J., and Wright, S., 2000, "Faster Top Running Speeds are Achieved With Greater Ground Forces not More Rapid Leg Movements," J. Appl. Physiol. Respir. Environ. Exerc. Physiol., **89**(5), pp. 1991–1999.

[8] Gregorio, P., Ahmadi, M., and Buehler, M., 1997, "Design, Control, and Energetics of an Electrically Actuated Legged Robot," IEEE Trans. Syst. Man. Cybernet. Part B, **27**(4), pp. 626–634.

[9] Gabrielli, G., 1950, "What Price Speed?," Mech. Eng., **72**(10), pp. 775–781.